

UDC 535.42:543.422:541.45

PHASE FORMATION IN MIXED TiO₂—ZrO₂ OXIDES
PREPARED BY SOL-GEL METHOD© 2011 E. Krалева^{1*}, M.L. Saladino², R. Matassa³, E. Caponetti^{2,3}, S. Enzo⁴, A. Spojakina¹¹*Institute of Catalysis, Bulgarian Academy of Sciences, 1113 Sofia, Bulgaria*²*Dipartimento di Chimica "S. Cannizzaro", Università di Palermo and INSTM-Udr Palermo, Parco d'Orleans II Viale delle Scienze pad 17, 90128 Palermo, Italy*³*Centro Grandi Apparecchiature-UniNetLab, Università di Palermo, Via F. Marini 14, 9018 Palermo, Italy*⁴*Dipartimento di Chimica, Università di Sassari and INSTM-Udr Sassari, Via Vienna 2, Sassari 07100, Italy**Received September, 17, 2010*

Pure titania, zirconia, and mixed oxides (3—37 mol.% of ZrO₂) are prepared using the sol-gel method and calcined at different temperatures. The calcined samples are characterized by Raman spectroscopy, X-ray powder diffraction, scanning electron microscopy, transmission electron microscopy, and nitrogen adsorption porosimetry. Measurements reveal a thermal stability of the titania anatase phase that slightly increases in the presence of 3—13 mol.% of zirconia. Practically, the titania anatase-rutile phase transformation is hindered during the temperature increase above 700 °C. The mixed oxide with 37 mol.% of ZrO₂ treated at 550 °C shows a new single amorphous phase with a surface area of the nanoparticles double with respect to the other crystalline samples and the formed srilankite structure (at 700 °C). The anatase phase is not observed in the sample containing 37 mol.% of ZrO₂. The treatment at 700 °C causes the formation of the srilankite (Ti_{0.63}Zr_{0.37}O_x) phase.

Key words: TiO₂—ZrO₂ mixed oxides, sol-gel method, srilankite, Rietveld method.

INTRODUCTION

Metal oxide nanostructures have been the focus of intensive research due to their potential application as catalysts for photodecomposition, semiconductor, water treatment materials and so on [1]. Titania (TiO₂) is widely used in various fields of applications because of its interesting and unique properties. Titania is known to have several natural polymorphs: rutile is thermodynamically stable, but anatase is metastable at low temperatures, and brookite is formed only under hydrothermal conditions [2]. Titania in the anatase form appears to be the most practical photocatalyst among the semiconductors for widespread environmental application because of a relatively high activity, chemical stability, low cost, and non toxicity. Even so, a slow reaction rate and poor solar efficiency have hindered its further applications. In order to enhance its application and the photocatalytic property, much attention has been paid in the recent years to modify TiO₂ by different methods such as establishing junctions between titania and other semiconductors [1, 2], doping with metals or ions [3—5], and composite design with porous materials [6—8]. ZrO₂ is an *n*-type semiconductor with the physicochemical properties similar to those of TiO₂; it is widely used in ceramics technology and heterogeneous catalysis.

Much attention has been focussed on the investigation of the synthesis of mixed ZrO₂—TiO₂ oxides and its relationship with the physicochemical and catalytic properties. It is known that the optimal efficiency of mixed oxide systems significantly depends on the method of their preparation. Many authors prepared TiO₂ doped with ZrO₂ using various methods, such as sol-gel [9, 10], polymer gel

* E-mail: e_kraleva@yahoo.com

templating [11], homogeneous co-precipitation [3], and hydrothermal synthesis [12]; and higher catalytic activity was found in comparison with pure TiO₂ in different reactions. An increase in the surface acidity, surface area, and oxygen vacancy defects are thought to be responsible for the enhanced activity. Control of the morphological properties of materials during synthesis is of paramount importance because these structural characteristics strongly affect their performances and purposes. For the ZrO₂/TiO₂ system, its catalytic properties are well known to be sensitive to the composition and structural properties. The binary solid solution is usually synthesized by the solid-state reaction of a ZrO₂ and TiO₂ mixture at a very high temperature (above 1400 °C) [13]. However, the material synthesized at the high temperature does not have a high surface area. The binary solid oxide can be obtained at much lower temperatures by the sol-gel method [14]. In the preparation of binary or multi-component oxide solid solutions by the sol-gel method, the key is to control the hydrolysis and condensation rates of the various molecular precursors used. The difference in reactivity can be minimized by controlled prehydrolysis of the less reactive precursor or by chemical modification of the precursors. The preparation of binary TiO₂—ZrO₂ solid by the sol-gel method has been reported [15, 16]. The sol-gel methods are very often used to prepare these mixed oxide coatings because it is a relatively low-cost process with inexpensive equipments and it could be easily converted to the industrial scale.

The aim of the current work was to prepare TiO₂—ZrO₂ oxides with a different ZrO₂ quantity (3—6—13—37 mol.%) using the sol-gel method. The morphological and structural properties of these binary TiO₂—ZrO₂ oxides were systematically investigated as function of the ZrO₂ quantity after calcination at two temperatures (550 and 700 °C) and were compared with the properties of pure titania and pure zirconia to determine the effect of the Zr content on the physicochemical properties of TiO₂. The phase composition, structure, morphology, and surface properties of the samples were studied with a multitechnique approach using X-ray powder diffraction (XRD), Raman spectroscopy, and transmission electron microscopy (TEM), X-ray fluorescence (XRF), and nitrogen adsorption porosimetry.

EXPERIMENTAL

Materials. Zr(OCH₂CH₂CH₃)₄ (zirconium(IV) propoxide, Aldrich) and Ti(OCH₂CH₂CH₃)₄ (titanium(IV) propoxide, Aldrich), were the sources of Zr⁴⁺, Ti⁴⁺ ions. CH₃CH₂CH₂OH (2-propanol, Merck), and NH₄OH (ammonia solution, Merck) were used as received.

Preparation of the TiZrn oxides. Pure TiO₂, pure ZrO₂ and binary samples (3, 6, 13 and 37 mol.% of ZrO₂ in samples) were prepared using the sol-gel method. The precursors Zr(OCH₂CH₂CH₃)₄ and Ti(OCH₂CH₂CH₃)₄ were partially hydrolyzed at 18 °C in 2-propanol with adding the ammonia solution and maintaining the pH equal to 9. After 5 min, the temperature was increased to 27 °C and an appropriate amount of deionized water was added dropwise at reflux for 1 h to complete the hydrolysis. The alcoxides:2-propanol:water:ammonia molar ratio was 1:4:1:0.33. The gels were aged *in situ* for 24 h and the residual liquid was removed by decanting. The xerogels were obtained after heating in an oven at 100 °C for 24 h in static air using a temperature ramp of 5 °C/min. Then, the samples were treated at 550 and 700 °C for 5 hours. The labels of the different binary samples will be referred as TiZrn, where Ti = TiO₂, Zr = ZrO₂, and *n* = 3, 6, 13, 37 mol.% of ZrO₂.

Characterization techniques. X-ray powder diffraction patterns were recorded in the 20—140° 2θ range at steps of 0.03° and a counting time of 3 s/step on a Philips PW 1050 diffractometer, equipped with a Cu tube and scintillation detector beam. The X-ray generator worked at 40 kV and 30 mA. The instrument resolution (divergent and antiscatter slits of 0.5°) was determined using standards free from the effect of reduced crystallite size and lattice defects. Diffraction patterns were analyzed according to the Rietveld method [17] using the MAUD program [18].

Raman spectra were collected at room temperature using Renishaw inVia Raman Microscopes operating with a 632.8 helium-neon laser and equipped with a Leica microscope. The signal was detected by means of a high sensitivity ultra-low noise cooled charge coupled detector (CCD), with a spectral resolution of 2 cm⁻¹.

Transmission Electron Microscopy study was performed using a JEM-2100 (JEOL, Japan) operating at 200 kV accelerating voltage, equipped with an energy dispersive X-ray spectrometer (EDS) (Oxford Instrument, UK) suited for element identification. The powder was sonicated in isopropanol to ensure a homogeneous dispersion. A small drop was deposited on the holey carbon films on a 200 mesh copper grid, which was introduced into the TEM analysis chamber after complete solvent evaporation.

Nitrogen adsorption-desorption isotherms were recorded at 77 K using a Quantachrome Nova 2200 Multi-Station High Speed Gas Sorption Analyzer. Samples were outgassed for 3 h at 573 K in the degas station. Adsorbed nitrogen volumes were normalized to the standard temperature and pressure. The specific surface area (S_{BET}) was calculated according to the standard BET method [19] in the relative adsorption pressure (P/P_0) range from 0.045 to 0.250.

RESULTS AND DISCUSSION

The XRD patterns of pure TiO_2 and ZrO_2 samples treated at 550 and at 700 °C are reported in Fig. 1 as $I(Q) \cdot Q$ vs 2θ where $Q = 4\pi/\lambda \sin(\theta)$ is the scattering vector. Experimental data points are matched with full lines calculated after Rietveld refinement. The bar sequence at the bottom refers to the peak positions expected from space group symmetry and atomic positions in anatase, rutile, monoclinic baddeleyite, and tetragonal zirconia cells respectively. It can be seen that the TiO_2 product obtained after treatment at 550 °C is constituted by a mixture of anatase and rutile in the wt. % proportion as 44:56. The lattice parameters of both rutile [S.G. $P4_2/mnm$, $a = 4.590(\pm 1)$ and $c = 2.957(\pm 1)$ Å, $Z = 2$] and anatase [S.G. $I4_1/amd$, $a = 3.782(\pm 1)$ and $c = 9.507(\pm 1)$ Å, $Z = 4$] gives the unit cell volumes, and hence the molar volumes, slightly lower than in the reference crystalline phases ($a = 4.5937$; 2.9587 for rutile and $a = 3.784$ Å and $c = 9.515$ Å for anatase respectively). The average crystallite size (i.e., of the coherently diffracting domain) is ca 320 Å (± 20) for anatase and 450 Å (± 30) for rutile.

It should be maintained that this figure is retrieved after a separation of size broadening from the strain according to an automatic procedure incorporated in the MAUD software. The same specimen heated at 700 °C shows that most of the powder has transformed to rutile (98 wt. %, $a = 4.592(\pm 1)$ Å; $c = 2.959(\pm 1)$ Å), with a consistent growth of crystallites whose average size is ca. 850 Å.

The XRD patterns of ZrO_2 sample subjected to the same thermal treatment of TiO_2 shows indirectly a high level of background, likely related to the fluorescence of zirconium atoms, which is witnessed by an ascending trend of the patterns when plotted as $\log[I(Q) \cdot Q]$ vs 2θ . A mixture of tetragonal and monoclinic polymorphic structures is now highlighted in this system. At 550 °C zirconia appears mainly in tetragonal geometry (76 wt. %), $P4_2/nmc$ space group, $a = 3.593$; $c = 5.173$. These values give a molar volume of 33.40 \AA^3 , slightly superior to 33.23 \AA^3 reported by Yashima and Tsune-

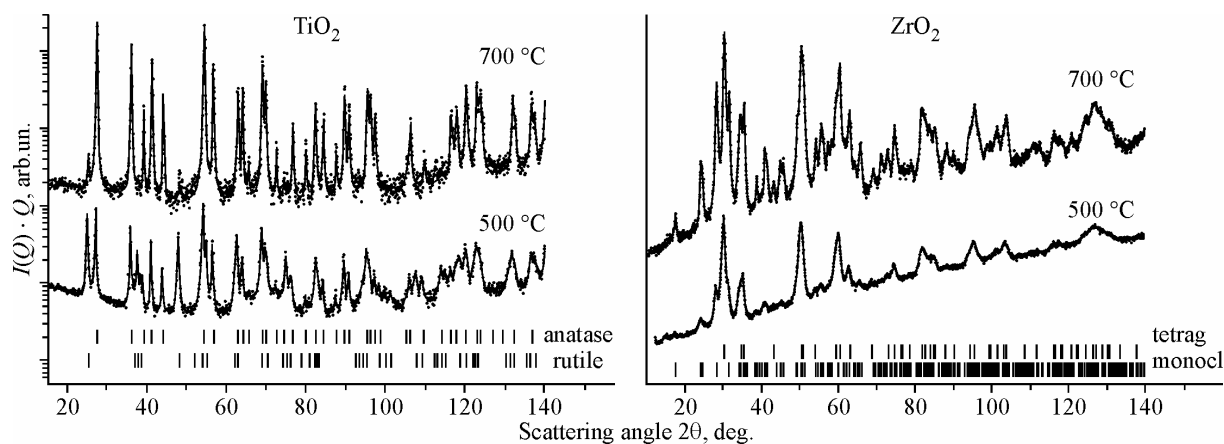


Fig. 1. XRD patterns and the Rietveld fits (dots and full lines respectively) of TiO_2 and of ZrO_2 samples treated at 550 and at 700 °C. At the bottom: bar sequence of reference patterns

kawa in nominally pure ZrO₂ after drying the ethanol sol in air on a quartz plate at 398 K for 22 h [20]. The line broadening analysis has revealed that for both phases the average grain size is as low as 150 Å with the average strain density of ca 0.003. The monoclinic baddeleyite form at 550 °C ($P2_1/c$ space group, $a = 5.140$, $b = 5.190$; $c = 5.317$; $\beta = 99.12^\circ$) gives a monoclinic molar volume of 35.01 Å³, relatively in keeping with the results of Yashima and Tsunekawa. At 700 °C the baddeleyite ZrO₂ form has increased its presence to ca 44 wt. %. Also the molar volume of 35.12 Å³ appears to be increased, together with the average grain size, which now holds approximately 270 Å. As for the remaining 56 wt. % of the tetragonal form, a similar behaviour is found. In fact, the molar volume increases to 33.52 Å³ and so it is for the average crystallite size (230 Å). No appreciable changes of the lattice strain density are detected at this stage.

The diffraction pattern of TiZr6 and TiZr13 samples treated at 700 °C are reported in Fig. 2. Contrary to pure titania treated at 700 °C, which was almost entirely in the rutile form, the TiZr13 specimen is a mixture of three phases, namely anatase (66 wt. %), rutile (19 wt. %) and orthorhombic (15 wt. %) srilankite type (S.G. $Pbcn$, $Z = 4$). Whether this is the third polymorph of TiO₂ (so-called high-pressure TiO₂ II form) or real srilankite phase is difficult to distinguish from the values of the lattice parameters. In fact, the data from the best fit turns out to be $a = 4.597$; $b = 5.714$, $c = 4.910$ Å, which is different from both the literature values for TiO₂ II ($a = 4.515$; $b = 5.497$; $c = 4.939$) and TiZrO₄ ($a = 4.806$; $b = 5.447$; $c = 5.032$). Thus, the addition of ZrO₂ to TiO₂ makes the maximum intensity of diffraction peaks to diminish due to the reduction of the average crystallite size and an increase in the lattice strain, generally referred to as a loss of crystallinity in the mixed oxides. In fact, the anatase average grain size is 230 Å with a lattice strain density of 0.0034. Observing the refined lattice parameters of anatase $a = 3.796(\pm 1)$ Å and $c = 9.564(\pm 1)$ Å it seems that there is a consistent volume cell expansion, affecting mainly the c axis (increase of 0.6 %) with respect to a and b (increase of ca 0.4 %). Since the radius of the Zr⁴⁺ ion (0.77 Å) is higher than the radius of the Ti⁴⁺ ion (0.60 Å), the replacement of Ti⁴⁺ ions in sites 4 (a) of the anatase structure by Zr⁴⁺ is expected to increase the unit cell volume. The resulting calculated molar volume of 34.45 Å³ is comparable with the value of 34.06 Å³ known from pure, undoped, anatase. Actually, the octahedrally distorted environment around titanium in pure anatase is composed by four Ti—O distances of 1.935 Å approximately in a plane

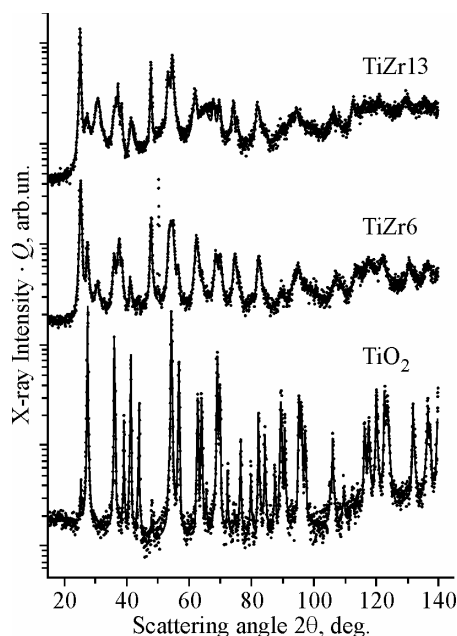


Fig. 2. XRD pattern and the Rietveld fits (dots and full lines respectively) of TiO₂, TiZr6 and TiZr13 samples treated at 700 °C

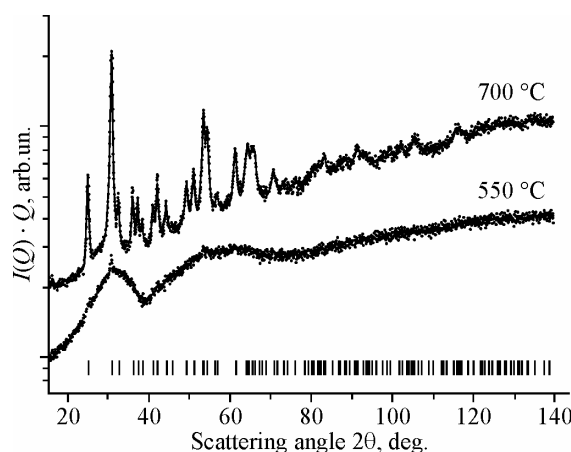


Fig. 3. XRD patterns and the Rietveld fits (blue dots and red full lines respectively) of TiZr37 samples treated at 550 and 700 °C. At the bottom: bar sequence of the orthorhombic Srilankite phase

parallel to the basal (a , b) plane and two Ti—O distances of 1.98 Å parallel to the c -axis. These figures become 1.94 Å and 1.99 Å respectively for the TiZr6 specimen. The rutile phases turn out to have the unit cell volume close to the literature values, but this is not so for the srilankite-type phase. The polymorphism may be an expression of the metastable energy conditions affected by this composition.

The situation changes after the addition of 13 mol.% ZrO₂. TiO₂ in the anatase form is again well recognized, with a further expansion of the lattice parameters to $a = 3.808$ Å; $c = 9.635$ Å, meaning a molar volume of 34.93 Å³. Simultaneously, the octahedral distribution of oxygen ions around 4 (a) sites of mixed (Ti, Zr) metal ions is described by four M—O nearest neighbour distances of 1.95 Å and two M—O distances of 2.005 Å. The average crystallite size of the anatase phase increases to 340 Å, but the amount of the srilankite-type phase increases to 40 %, while its cell parameters remain essentially unchanged with respect to the TiZr6 specimen. The diffraction patterns of TiZr37 samples treated at 550 and 700 °C are reported in Fig. 3 and show another structural behaviour.

The XRD pattern of the TiZr37 sample shows that the specimen treated at 550 °C is almost completely amorphous, confirming the previous general observation of a crystallinity loss as a function of zirconium addition to the Ti-based precursor. Note in any case that weak traces of an orthorhombic phase (amounting to less than 0.5 wt. %) are appreciable. After the treatment at 700 °C the whole amorphous component is transformed into the Srilankite oxide, with the lattice parameters $a = 4.705$, $b = 5.525$, $c = 4.997$ Å, again consistently different from the previously reported literature values for TiZrO₄. Our experimental data are closer to the values measured by Willgallis and Hartl [21] for Ti_{0.67}Zr_{0.33}O₂. This structure accounted well for the experimental data points with a Rietveld fit, as shown by the red full line, which includes also the peak broadening behavior giving an average crystallite size of ca. 205 (±10) Å and an average lattice strain of 0.0024 (±0.0004). Note also that Sham et al. [22] have studied the amorphous-to-crystalline transformation of zirconium titanate from the sol-gel synthesis after heating at 1000 °C, using the Rietveld method. The samples were mixtures of TiO₂, Zr₅Ti₇O₂₄, and ZrO₂ oxides, and the stoichiometry of the stable zirconium titanate phase was found to be Zr₅Ti₇O₂₄ rather than ZrTiO₄ (Zr₆Ti₆O₂₄).

The Raman spectra of TiZr n samples treated at 550 and 700 °C are shown in Fig. 4. There are six active bands (A1g + 2B1g + 3Eg) reported in the literature for anatase, namely, at 144 cm⁻¹ (Eg), 197 cm⁻¹ (Eg), 399 cm⁻¹ (B1g), 513 cm⁻¹ (A1g), 519 cm⁻¹ (B1g), and 639 cm⁻¹ (Eg). Actually, the two

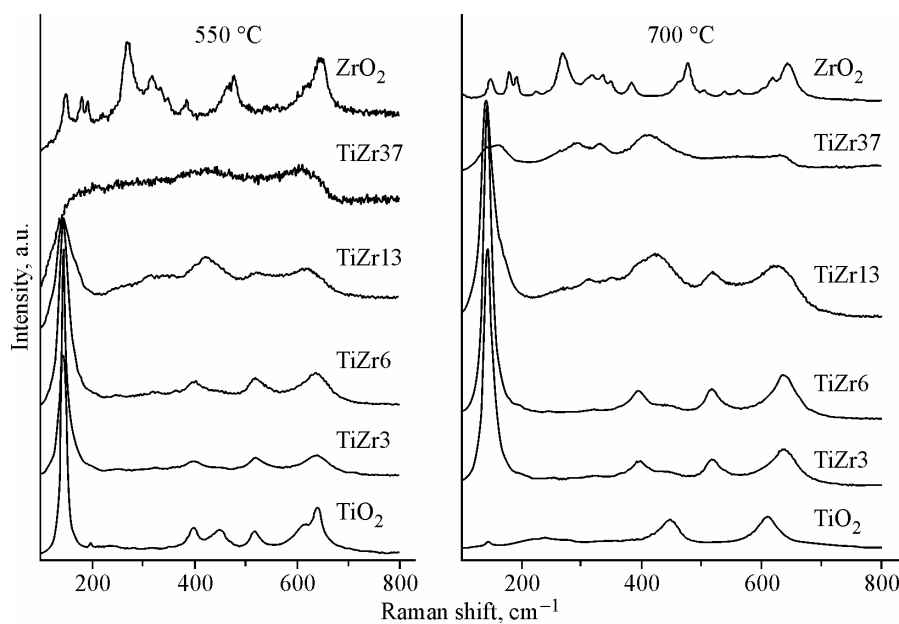


Fig. 4. Raman spectra of TiZr n samples treated at 550 and 700 °C

bands at 513 cm⁻¹ and 519 cm⁻¹ are very close. Omitting the very weak band at about 197 cm⁻¹, we can assume that the bands at 144.6 cm⁻¹, 397.7 cm⁻¹, 518.8 cm⁻¹, and 640.0 (±0.1) cm⁻¹ are indicative of the anatase presence, while the three other broad features located approximately at 236 cm⁻¹, 444 cm⁻¹, and 610 cm⁻¹ respectively are from the rutile phase.

Conversely, the top curve of the lhs graph reports the spectrum of ZrO₂ which shows mainly the characteristic bands of the monoclinic baddeleyite and tetragonal ZrO₂ polymorphous phases at about 181 cm⁻¹, 190 cm⁻¹, 222 cm⁻¹, 310 cm⁻¹, 337 cm⁻¹, 382 cm⁻¹, 474 cm⁻¹, 499 cm⁻¹, 540 cm⁻¹, 559 cm⁻¹, 620 cm⁻¹, and 636 cm⁻¹ [23].

The Raman spectra of the TiZr n samples with $n = 3$ and 6 show the bands wider than those of pure TiO₂ around 144 cm⁻¹, 397 cm⁻¹, 518 cm⁻¹, and 638 cm⁻¹, which are characteristic of the anatase phase. The bands of the anatase phase are further broadened in the Raman spectrum of the TiZr13 sample and their relative intensities are significantly different from those of specimens with a lower Zr content. This behavior can be due to the presence of local atomic disorder in the anatase lattice caused by the formation of the Ti—O—Zr bond. In addition, a broad feature emerges centred at ca. 430 cm⁻¹ that needs a careful explanation. The 430—440 cm⁻¹ band could be either a rutile peak shifted by about 10 cm⁻¹ to a lower wavenumber or an anatase peak shifted by about 30 cm⁻¹ to higher wavenumber. However, some authors assigned this peak to the tetragonal phase of zirconia [17]. These possibilities will be checked in the following by XRD.

The TiZr37 specimen does not show the bands ascribable to the presence of the symmetric environment and thus very likely refers to a sample in the amorphous condition.

The Raman spectra of TiZr n samples treated at 700 °C are shown in Fig. 4. Here the Raman spectrum of the pure TiO₂ sample exhibits bands at about 240 cm⁻¹, 442 cm⁻¹, and 606 cm⁻¹, typical of the rutile phase. The pure ZrO₂ spectrum still shows the baddeleyite characteristic bands. This comparison highlights the different stability of the sol-gel prepared powders of two pure components. Conversely, the Raman spectra of TiZr3 and TiZr6 samples treated at 700 °C show the bands of the anatase phase, with a weak band at 450 cm⁻¹ attributable to the presence of rutile. It seems that the addition of zirconium atoms relatively stabilized the anatase phase. The Raman spectrum of the TiZr13 sample also shows broad bands of the anatase phase with a more evident broad band at 421 cm⁻¹ that may be the effect of rutile as well as another type of interaction at the atomic level. Finally, the broad bands in the spectrum of TiZr37 are attributed to the *srilankite* phase.

HR-TEM micrographs of TiO₂ and of ZrO₂ treated at 700 °C are reported in Fig. 5.

Both titania and zirconia are constituted by flattened clusters of nanoparticles having defined boundaries with a polygonal-like shape. Titania particles have a size of about 50 nm wide and 110 nm long.

Conversely, the TiZr6 sample micrograph, reported in Fig. 6, shows a mixture of 20 nm particles of different shapes indicating the presence of many crystalline phases. The cubic and spherical shapes are indicative of rutile and anatase phases respectively.

TEM micrographs at different magnification of the **TiZr37** sample treated at 550 and 700 °C are reported in Fig. 7.

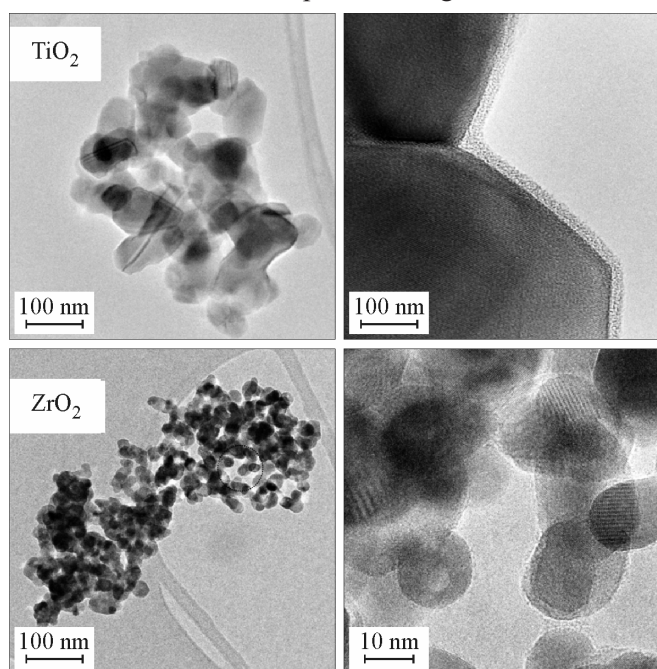


Fig. 5. HR-TEM micrographs of TiO₂ and ZrO₂ samples treated at 700 °C

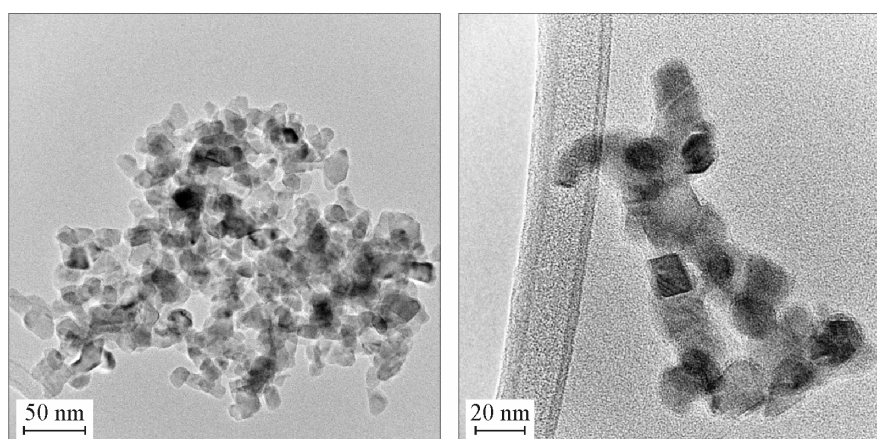


Fig. 6. HR-TEM micrographs of TiZr6 sample treated at 700 °C

TEM micrographs of the TiZr37 sample treated at 550 °C show snowflake aggregate networks of small nanoparticles having the spheroid shape and the crystallite size around 10 nm, which is a typical image of amorphous oxide. In some point of the powder, small nanocrystals of the srilankite phase are present in agreement with the XRD analysis results. The TEM micrographs of the TiZr37 sample treated at 700 °C show aggregated particles with a not well-defined shape. The spherical particles are interconnected between them.

The shapes of all the isotherms are similar regardless of the Zr quantity and thermal treatment. All of the nitrogen adsorption—desorption isotherms show a slow increase in the adsorbed amount of N_2 . According to the IUPAC classification, the N_2 adsorption isotherms of the samples can be identified as type IV with an H3 type hysteresis loop [24] suggesting the existence of mesoporous structures in the resulting materials. The ZrO_2 isotherm exhibits Type II behavior. An indication for microporosity was not obvious in the isotherms measured at low relative pressures. Thus, the materials consist of agglomerates of very small primary particles, as evidenced by the electronic micrographs. Some degree of mesoporosity is evident from the hysteresis and can be attributed to the interparticle porosity or the presence of mesopores. As an example, N_2 adsorption and desorption isotherms of TiO_2 and of TiZr37 treated at 550 and 700 °C are reported in Fig. 8.

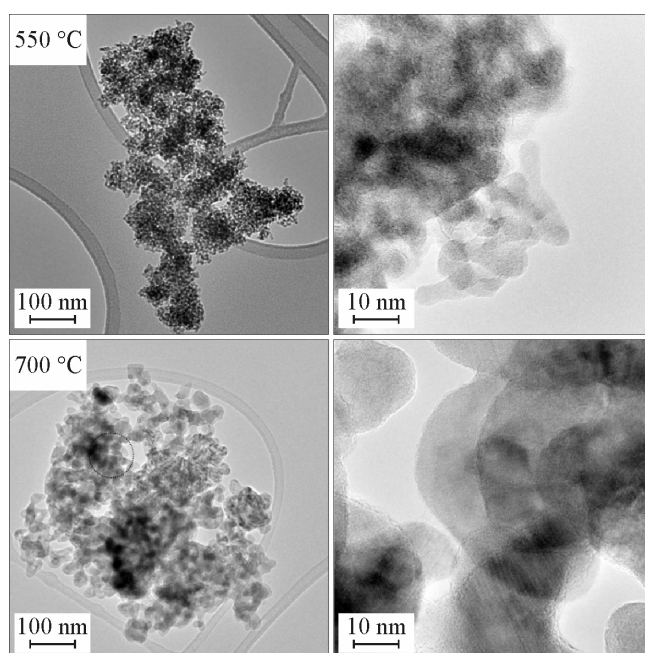


Table 1
BET surface area of TiZrn samples treated at 550 and 700 °C

Sample	ZrO ₂ (mol.%)	S_{BET} (m ² /g)	
		550 °C	700 °C
TiO ₂	0	22	19
TiZr3	3	26	26
TiZr6	6	37	29
TiZr13	13	40	30
TiZr37	37	172	36
ZrO ₂	100	42	28

Fig. 7. HR-TEM micrographs of TiZr37 samples treated at 550 and 700 °C

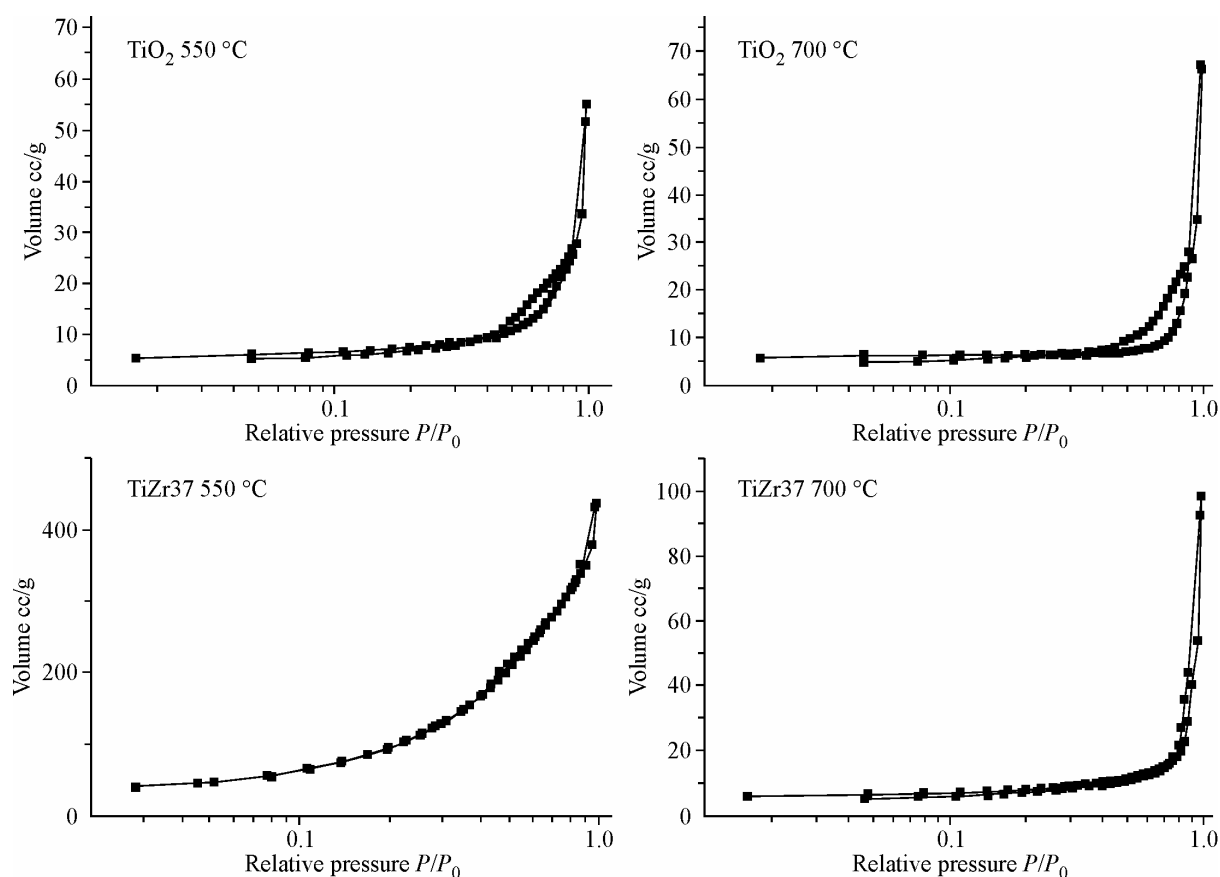


Fig. 8. N₂ adsorption and desorption isotherms of TiO₂, and of TiZr37 samples treated at 550 and 700 °C

The BET specific surface area (S_{BET}) of the samples was calculated from the N₂ adsorption isotherms in the 0.045—0.250 relative pressure range. The results are reported in Table 1.

The surface area slowly increases with increasing zirconia quantity. The TiZr37 sample treated at 550 °C presents a larger surface area with respect to the other samples. We remind that both XRD and Raman data (supported by TEM micrographs) showed that this sample is in an amorphous condition. Therefore, it is clear that if the concentration of ZrO₂ increases up to 37 mol.% at 550 °C, it is more difficult for the system to crystallize. As the temperature increases to 700 °C, the crystallization of srilankite occurs with a consequent surface area decrease.

CONCLUSIONS

TiO₂—ZrO₂ samples were prepared using the sol-gel method. The XRD patterns and Raman spectra showed that the addition of zirconia affects the formation and quantity ratio of the polymorphous phases of TiO₂ and ZrO₂. Specifically, the ZrO₂ addition to TiO₂, equivalent to 6 mol.% and 13 mol.%, involves the partial Ti⁴⁺ substitution for Zr⁴⁺ ions with an expansion of the anatase lattice parameters with respect to the pure anatase phase. This expansion is slightly more evident along the *c* axis. It is related to a distance increase in the distorted octahedral oxygen ions surrounding the metal ions in the anatase lattice. The single and mixed oxides showed morphologies constituted by microspheroid aggregates independently of the TiO₂/ZrO₂ molar ratio and the crystalline structure, indicating a homogeneous kinetics of the nucleation of microspheroids during the synthesis.

The mixed oxide with 37 mol.% of ZrO₂ treated at 550 °C shows a new single amorphous phase with a surface area of the nanoparticles double with respect to the other crystalline samples, and the srilankite structure (at 700 °C) formed. The anatase phase was not observed in the sample containing 37 mol.% of ZrO₂. The treatment at 700 °C causes the formation of the srilankite (Ti_{0.63}Zr_{0.37}O_x) phase.

The N₂ adsorption measurements showed that the powders contain some mesoporous characteristics and the surface area increases with the Zr quantity. The amorphous TiZr37 sample treated at 500 °C is the only sample with a large surface area.

Acknowledgments. This work was made with the support of the Bulgarian Ministry of Education, Fund "SCIENTIFIC RESERCH" (project № DO1-900/24.11.07). E. K is indebted to the M.E. for a postdoctoral grant in the Chemical-Physic Department, University of Palermo (Italy). The present work is a part of the joint project between the Institute of Catalysis, Bulgarian Academy of Sciences and the Institute of Chemical Process Fundamentals, Academy of Sciences of the Czech Republic. The authors would like to thank the MIUR for supporting this research through the PRIN 2007 prot. 20077R3PXF_002 "New nanocomposites preparation for optical, electric and magnetic applications". TEM experimental data were provided by Centro Grandi Apparecchiature—UniNetLab—Università di Palermo funded by P.O.R. Sicilia 2000—2006, Misura 3.15 Azione C Quota Regionale.

REFERENCES

1. Hernandez-Alonso M.D., Tejedor-Tejedor I., Coronado J.M. et al. // *Thin Solid Film.* – 2006. – **50.** – P. 2125 – 2131.
2. Aguado J., van Grieken R., Lopez-Munoz M.-J., Marugan J. // *Appl. Catal. A: Gen.* – 2006. – **312.** – P. 202 – 212.
3. Luka J., Klementova M., Bezdzicka P. et al. // *Appl. Catal. B: Environ.* – 2007. – **74.** – P. 83 – 91.
4. Wang Y.M., Liu S.W., Lu M.K. et al. // *J. Mol. Catal. A: Chem.* – 2004. – **215.** – P. 137 – 142.
5. Djerdj I., Arcon D., Jaglicic Z., Niederberger M. // *J. Solid State Chem.* – 2008. – **181.** – P. 1571 – 1581.
6. Anandan S., Yoon M. // *J. Photochem. Photobiol. C: Photochem.* – 2003. – **4.** – P. 5 – 18.
7. Jitianu A., Cacciaguerra T., Benoit R. et al. // *Carbon.* – 2004. – **42.** – P. 1147 – 1151.
8. Torimoto T., Okawa Y., Takeda N. et al. // *Photobiol. A: Photochem.* – 1997. – **103.** – P. 153 – 157.
9. Fu X.Z., Clark L.A., Yang Q., Anderson M.A. // *Environ. Sci. Technol.* – 1996. – **30.** – P. 647 – 653.
10. Colon G., Hidalgo M.C., Navio J.A. // *Appl. Catal. A: Gen.* – 2002. – **231.** – P. 185 – 199.
11. Schattka J.H., Shchukin D.G., Jia J. et al. // *Chem. Mater.* – 2002. – **14.** – P. 5103 – 5108.
12. Hirano M., Nakahara C., Ota K. et al. // *J. Solid State Chem.* – 2003. – **170.** – P. 39 – 47.
13. Isobe T., Komatsubara S., Senna M. // *Nippon Kagaku Kaishi.* – 1991. – P. 1361.
14. Isobe T., Komatsubara S., Senna M. // *J. Non-Cryst. Solids.* – 1992. – **150.** – P. 144 – 147.
15. Twesme T.M., Tompkins D.T., Anderson M.A., Root Th.W. // *Appl. Catal. B: Environmental.* – 2006. – **64.** – P. 153 – 160.
16. Youl J.K., Bin P.S. // *Korean Journal of Chemical Engineering.* – 2001. – **18,** N 6. – P. 879 – 888.
17. Young R.A. Ed. *The Rietveld Method.* – Oxford: University Press, 1993.
18. Lutterotti L., Gialanella S. // *Acta Mater.* – 1998. – **46.** – P. 101 – 110.
19. Brunauer S., Emmett P.H., Teller E. // *J. Amer. Chem. Soc.* – 1938. – **60.** – P. 309 – 315.
20. Yashima, Tsunekawa // *Acta Cryst. B.* – 2006. – **62.** – P. 161 – 164.
21. Willgallis A., Hartl H. // *Zeitschr Kristallogr, Crystal Research, Technology.* – 1989. – **24,** N 3. – P. 263 – 268.
22. Sham Edgardo L., Aranda Miguel A.G., Farfan-Torres E. Mynica et al. // *J. Solid State Chem.* – 1998. – **139.** – P. 225 – 232.
23. Kyeong Youl Jung, Seung Bin Park // *Materials Lett.* – 2004. – **58.** – P. 2897 – 2900.
24. Beattie I.R., Gilson T.R. // *J. Chem. Soc. A.* – 1969. – P. 2322 – 2329.